THE JOURNAL OF PHYSICAL CHEMISTRY C

C: Physical Processes in Nanomaterials and Nanostructures

Towards Controlled Synthesis of Water-Soluble Gold Nanoclusters: Synthesis and Analysis

Karolina Sokolowska, Sami Malola, Manu Lahtinen, Ville Saarnio, Perttu Permi, Katariina Koskinen, Matti Jalasvuori, Hannu Häkkinen, Lauri Lehtovaara, and Tanja Lahtinen

J. Phys. Chem. C, **Just Accepted Manuscript** • Publication Date (Web): 07 Jan 2019

Just Accepted

ACS Publications

is published by the American Chemical Society. 1155 Sixteenth Street N.W., Washington, DC 20036

Towards Controlled Synthesis of Water-Soluble Gold Nanoclusters: Synthesis and Analysis

Karolina Sokołowska [1], Sami Malola [2], Manu Lahtinen [1], Ville Saarnio [1], Perttu Permi [1,3], Katariina Koskinen [3], Matti Jalasvuori [3], Hannu Häkkinen [1,2], Lauri Lehtovaara [1] and Tanja Lahtinen [1].*

1 Department of Chemistry, Nanoscience Center, University of Jyväskylä, P.O. Box 35, 40014 Jyväskylä, Finland

2 Department of Physics, Nanoscience Center, University of Jyväskylä, P.O. Box 35, 40014 Jyväskylä, Finland

3 Department of Biological and Environmental Science, Nanoscience Center, University of Jyväskylä, P.O. Box 35, 40014 Jyväskylä, Finland

ABSTRACT: Water-soluble gold nanoclusters with well-defined molecular structure and stability possess particular biophysical properties making them an excellent candidate for biological application as well as for fundamental spectroscopic studies. The currently existing synthetic protocols for atomically monodisperse thiolate-protected gold nanoclusters (AuMPCs) have been widely expanded with organothiolates yet the direct synthesis reports for water-soluble AuMPCs are still deficient. Here, we demonstrate a wet-chemistry pH controlled synthesis of two large water-soluble nanoclusters utilizing *p*-mercaptobenzoic acid (*p*MBA), affording different sizes of plasmonic AuMPC on preparative scale (~7 mg). AuMPCs are essentially homogenous in size and are stable in solution and solid state. Number of characterization methods were used to gain detailed information about the size, symmetry, molecular composition and structure of these systems: i.e. HR-TEM, Powder X-ray Diffraction (PXRD), NMR, UV-Vis,

Thermogravimetry (TG) and PAGE (Polyacrylamide Gel Electrophoresis). Based on the conducted experimental analyses and computationally aided predictions it can be evidenced that both clusters exhibit twinned FCC symmetry with the molecular composition of $Au_{210\text{-}230}(p\text{MBA})_{70\text{-}80}$ and $Au_{426\text{-}442}(p\text{MBA})_{112\text{-}115}$; referred from now on as Au250 and Au500, respectively. For future reference, toxicity of both gold clusters in various concentrations on cultures of gram-positive and gram-negative bacteria was investigated.

1. INTRODUCTION

The unique properties of gold nanoparticles have been studied extensively.[1-4] The size and shape of the particles define their electronic and physical properties, whereas

tuning the nature of the protecting organic layer gives a control of the solubility and chemical functionality of the particles.[1] The versatile surface chemistry and size-dependent properties make them universal material in high technology applications such as sensory probes, electronic conductors, therapeutic agents, drug delivery in biological and medical applications, and catalysis.[4-11]

Colloidal nanoparticles are not well suited for accurate studies of their chemistry. A typical nanoparticle synthesis produces a polydisperse sample of different sizes, shapes, and surface structures. Therefore, experiments that require atomic-level control are extremely difficult to carry out. In this regard, monolayer protected gold clusters (AuMPCs) are small (usually < 2 nm) nanoparticles with well-defined structures, consisting of metallic core and protecting ligand layer.[12-14] The structures range from small more molecular-like species, with quantized electronic transitions, to larger more nanoparticle-like clusters with hundreds of metal atoms, exhibiting localized surface plasmon resonance.[3,15,16] Contrary to colloidal gold nanoparticles, AuMPC synthesis produces a well-organized structure, with a specific number of atoms, similar to a molecule that has enabled accurate studies of their chemistry, as well as direct

comparison of experimental and theoretical results.[17] Currently, many sizes of organosoluble nanoclusters are widely deployed;[18-23] however the direct syntheses of larger (> 200 gold atoms) water-soluble nanoclusters are still not yet fully understood.

Water-soluble gold nanoclusters were previously reported as universal labeling tools for the bioimaging due to contrast properties, low toxicity and high solubility. For example, $Au_{102}(p\text{MBA})_{44}$ was described as a good tracking candidate for accurate site-specific covalent conjugation to the viral capsid surface where the covalently bound nanoclusters keep the viruses stable, allowing better visualization of their entry in complex endosomal structures.[4] The surface properties, particularly the solvent/organic interface of *p*MBA-protected gold clusters, are altered depending on the protonation state of the cluster.[1] The clusters become water-soluble only when the carboxylic group of *p*MBA-ligand is deprotonated, which is important aspect for chemical modifications. Moreover, water-soluble clusters do not require any toxic solvent treatment, which makes them a good candidate for green chemistry approaches, and widen the range of applicability to more polar solvents.

AuMPCs have a great response to the light at resonant wavelength.[23,24] The plasmonic and near-infrared absorbance (NIR) is well detectable in deep-tissue samples. We have previously studied covalently bound multimers of gold nanoclusters and discovered that the examined system displays coupled plasmonic modes in the NIR therapeutic spectral window (650-1350 nm) which could be potentially used for imaging biological samples.[25] Ability to covalently link AuMPC through conductive molecule opens up new prospects to study fundamental physical properties of molecular electronic devices and internal motions of the particles and binding ligands.[26] Recently, Bürgi *et al.* reported successful assembly of $Au_{25}(SBut)_{18}$ multimers via ligand exchange and studied electron transfer between clusters.[27] Developments of larger precise analogs of structures that can be modelled with ab initio (DFT) level of theory could expand the knowledge of quantum plasmonics and emergence of bulk properties of metals.

Currently existing synthetic protocols for producing AuMPCs are most extensively carried out using organosoluble ligands; organothiolates, - in particular phenylethanethiol (PET).[18-22,30] The synthesis generally produces a set of

heterogeneous particles, requiring etching, size focusing and/or other methods to narrow size distribution.[18,27-33] The key, to the characteristic stability and the atomically precise size control of those particles is the role of protecting ligand layer. Covalently bound ligands govern the kinetic control and thermodynamic selection of the robust sizes in the synthesis.[3] In contrast to the AuMPCs, the colloidal gold nanoparticles are typically protected by weakly bound surfactant or even without any protecting ligand layer, significantly affecting their stability leading to extensive aggregation. For water-soluble gold nanoclusters, the synthetic control is obtained by precise selection of reaction conditions, in a way that the single sized product is favored.[34, 35] To produce a large panel of uniform clusters of chosen sizes, the synthetic parameters of these direct synthesis methods need to be explored thoroughly.[36] Among several water-soluble thiols that can stabilize gold nanoclusters, mercaptobenzoic acid (MBA) has been actively used.[31-41] More specifically, syntheses have been developed for 3-MBA (*m*MBA)[37-40] and 4-MBA (*p*MBA)[31-36,41,42] protected clusters; e.g. Au_{68}(*m*MBA)$_{32}$ Au_{144}(*m*MBA)$_n$ and Au_{144}(*p*MBA)$_{60}$, Au_{102}(*p*MBA)$_{44}$ and Au_{146}(*p*MBA)$_{57}$. Among *p*MBA-stabilized particles, only Au_{144}(*p*MBA)$_{60}$ and Au_{102}(*p*MBA)$_{44}$ were synthesized without

any size focusing methods, resulting in direct synthesis protocol. In this work, we are focusing on *p*MBA-stabilized gold nanoclusters to study synthetic parameters of direct synthesis methods.

Precise characterization of individual gold nanoclusters in respect to their composition and structure has been made by various techniques.[38,40,41] However, despite of significant development in structure determination techniques within past years, atomic-level information of clusters bigger than 100 gold atoms is still a grand challenge to achieve, particularly for water-soluble clusters. Thereby, with lack of information on structure-properties relationship applicability of the clusters remains limited.

In this paper, through the systematic variation of reaction conditions we synthesized stable, water-soluble *p*MBA-thiolate gold nanoclusters. We found that controlling the pH in different MeOH/H_2O conditions produces different sizes of *p*MBA-clusters. To our knowledge, this is the first straightforward wet-chemistry synthesis to produce larger, water-soluble *p*MBA-protected gold nanoclusters in milligram scale. Experimental and theoretical evidence helped us to predict molecular composition of these larger *p*MBA-clusters to be

$Au_{210\text{-}230}(p\text{MBA})_{70\text{-}80}$ and $Au_{426\text{-}442}(p\text{MBA})_{112\text{-}115}$ referred further on as Au250 (synthesis previously published by us)[25,42] and Au500, respectively. The synthesized clusters are stable both in solid and in solution at room temperature for at least six months, as determined by PAGE and UV-vis analysis. For future studies, the toxicity of both gold clusters was also studied. As a result, neither Au250 or Au500 caused significant decrease or elevation in the growth densities of *Bacillus thuringiensis* HER1410, *Escherichia coli* HB101 or *Klebsiella pneumonia*.

2. MATERIALS AND EXPERIMENTAL METHODS

Materials

All reagents were commercial and used as received unless otherwise mentioned.

Synthesis and separation

*p*MBA-thiol protected AuMPCs were synthesized under pH controlled conditions. Different solvent compositions were used to fine-tune the reduction kinetics of the MPC

growth leading to the discrete cluster size (Fig. 1). Smaller nanocluster Au250 was synthesized at higher pH (around 11) with mixed solvent of 26% MeOH (v/v) in water,[25] whereas larger nanocluster Au500 was synthesized at slightly lower pH (around 9) and having solvent mixture of 24% MeOH in water.

In a typical synthesis, $HAuCl_4$ first reacts with excess *p*MBA-thiol in basic aqueous solution to form colorless Au(I)SR aggregated complexes. Then, $NaBH_4$ is added to reduce Au(I)SR into $Au_x(pMBA)_y$. The synthesis of smaller Au250 nanocluster produces one single size of AuMPCs. Detailed description of the syntheses and purification are given in ESI.

Due to the lack of crystal structure, several characterization techniques were conducted to gain detailed information about the size, symmetry, molecular composition and structure of these systems. The as-obtained products were analyzed using polyacrylamide gel electrophoresis (PAGE), thermogravimetric analysis (TGA), powder X-ray diffraction (PXRD), nuclear magnetic resonance spectroscopy (NMR), high resolution-transmission electron microscopy (HR-TEM), UV-vis spectroscopy, and mass spectrometry. Unfortunately, all the attempts to measure ESI-MS have not been

successful most likely due to large amount of possible charge states of protective *p*MBA-ligand layer.

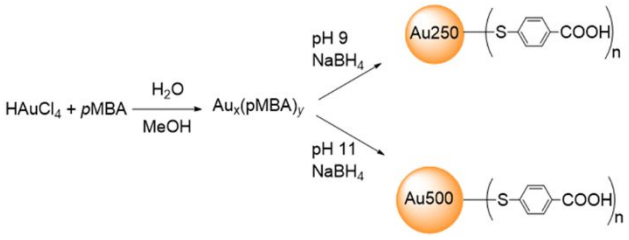

Scheme 1. Schematic representation of the gold nanocluster synthesis.

2.1. Polyacrylamide gel electrophoresis (PAGE). PAGE was run on a 15 % polyacrylamide gel (29:1 acrylamide:bisacrylamide) using 2X TBE run buffer in a Bio-Rad Mini-Protean Tetra System gel electrophoresis apparatus at 130 V.

Spectroscopy

2.2. Nuclear magnetic resonance (NMR). ^{1}H NMR spectra were recorded on a Bruker Avance III HD 800 MHz spectrometer, equipped with cryogenically cooled ^{1}H, ^{13}C, ^{15}N triple-resonance PFG Cryoprobe. All spectra were measured at 303 K.

2.3. UV-vis spectroscopy. The spectra of AuMPCs were measured in dH_2O using quartz cuvettes and Perkin Elmer Lambda 850 UV/Vis -spectrometer with 2 nm resolution.

2.4. Thermogravimetric analysis (TG). Thermal properties of Au-nanoclusters were examined by Perkin Elmer Pyris 1 thermogravimetric analyzer. TG runs were carried out in an open platinum pan under air atmosphere (flow rate of 60 ml/min) with a heating rate of 10 °C/min on temperature range of 20 − 800 °C. Analyses were made twice for each cluster type. Temperature calibration of the analyzer was made by using Curie transition temperatures of Alumel, nickel, Perkalloy and Fe standards. The weight balance was calibrated by measuring the standard weight of 50 mg at room temperature. The sample weights used in the measurements were about 1 – 3 mg.

2.5. Powder X-ray diffraction (PXRD) measurements. The powder X–ray diffraction data were measured by PANalytical X´Pert PRO diffractometer in Bragg–Brentano

geometry using Cu Ka1 radiation (Johannsson type monochromator; λ = 1.5406 Å) with 45kV and 40mA power settings. A sample was prepared on a reflection-free silicon-made plate with an aid of petrolatum jelly. Diffraction patterns were recorded from a spinning sample by X´Celerator detector using continuous scanning mode in 2θ range of 2 - 140° with a step size of 0.017° and with overall data recording time of ~ 45 h per pattern. Data processing was made with PANalytical HighScore Plus v. 4.7 program and phase identification data was retrieved from ICDD PD4+ database.[43] Theoretical powder diffraction curves were calculated as described in Ref. 44.

2.6. High Resolution-Transmission Electron Microscopy (HR-TEM). HR-TEM samples were prepared by drop-casting 8 µl of aqueous solution of clusters on a glow discharged 400 mesh lacey carbon copper grid. Solution was allowed to deposit for 15 min, after which excess sample was removed and washed with water and MeOH. Grid was allowed to dry overnight. Samples were imaged with 0.2 nm point resolution using JEOL JEM-2200FS Cs-corrected HR-TEM operated at 200 kV.

Simulated HR-TEM images were created from a cluster model with the following algorithm. A unit vector with random orientation was sampled from uniform angular

distribution. Each gold atom in the cluster model was replaced by a Gaussian density distribution with variance of 1.4 Å, and the density was projected onto the plane defined by the random unit vector. Finally, the resulting projected density was converted to grayscale image.

2.7. Prediction of the molecular composition. Computationally aided predictions of the molecular composition were done in three ways. In the first approach, theoretically calculated TG-percentages of the selected structurally known reference systems were correlated with the number of Au-atoms and the ligands in the systems. In the second approach, bare Au-cluster models of twinned FCC symmetry were used to estimate the number of metal atoms in the core of the synthesized clusters. In the third approach, compositions were predicted by using linear dependence of the number of gold atoms in the cluster to the volume of the cluster and also by the linear dependence of the number of ligands to the surface area of the cluster. More detailed information in ESI.

2.8. Bacteria/Toxicity test. Bacterial biotoxicity of Au250 and Au500 were spectroscopically determined against three bacterial species, *Bacillus thuringiensis* strain HER1410 (gram-positive), common lab-strain *Escherichia coli* K-12 HB101 (gram-

negative) and multidrug-resistant patient isolate *Klebsiella pneumoniae* (gram-negative). All strains were initially cultured in 5 ml of LB medium in + 37 °C and shaken 210 rpm overnight. Cultures for spectroscopic assay were prepared by adding aqueous solution of Au250 or Au500 in final concentrations of 0.14 μg/ml, 1.4 μg/ml, 14 μg/ml or 140 μg/ml and 0.13 μg/ml, 1.3 μg/ml, 13 μg/ml or 130 μg/ml, respectively, into 1:1000 diluted bacterial cultures. Absorbance of bacterial cultures were measured in + 37 °C at 595 nm in 5 minutes intervals for 20 hours in order to determine the bacterial growth and the maximum population densities. The absorption of Au250, Au500 and growth media was substracted from the maximum population densities to measure the bacterial cell induced absorption under different Au250 and Au500 exposures. Each measurement was conducted three times.

3. RESULTS AND DISCUSSION

3.1 Synthesis products. Two parameters, pH and MeOH concentration affected the outcome of the synthesis. Au nanoclusters were synthesized by pH control in different MeOH composition yielding two different discrete products of stable water-soluble

cluster protected by *p*MBA-thiol in milligram scale. These syntheses does not involve any additional size-focusing step and in case of Au250 the synthesis produces only one discrete size of particle. Additionally, $Au_{102}(pMBA)_{44}$ nanocluster was synthesized as a good reference point to compare synthetic trends, dispersity and size of the particles. The reference $Au_{102}(pMBA)_{44}$ nanocluster was synthesized following previously reported synthesis.[34] The polymerization step requires relatively high pH of ~13 and conditions of 47% of MeOH. To enable facile comparison of the reaction conditions, we divided the reaction protocols into 3 stages to extract the information on direct synthesis conditions. The first stage involves polymerization process, second stage reduction and the last one purification (Table 1).

To synthesize smaller Au250 nanoclusters, $HAuCl_4$ and *p*MBA-thiol were dissolved in methanol and mixed, leading to the formation of white precipitate. The initial $Au_x(pMBA)y$ polymerization step requires treatment at a pH of ~11 prior to reduction nucleating the growth of the metal core. After reduction of Au(I)-*p*MBA precursors with $NaBH_4$, excess of methanol is added and the reaction is quenched producing one discrete size of particle.

Lowering the pH, larger Au500 nanocluster was found. $HAuCl_4$ and *p*MBA-thiol were dissolved in 86 % of methanol forming rapidly white precipitate, which was dissolved at pH ~9. The final product still contains polydisperse clusters mixture, similar to the $Au_{102}(pMBA)_{44}$ synthesis, and requires fractional precipitation. The separation is done at 25 % of methanol and centrifuged at 5000 g for 15 mins. Next, the supernatant is adjusted to 80 % methanol and centrifuged. The pellet from precipitation at 80 % methanol is the final product.

The pH value of the *p*MBA-cluster effects its protonation state and surface properties. The solvent/organic interface of protecting ligand can be easily altered becoming water-soluble when the carboxylic group of *p*MBA-ligand is deprotonated and methanol-soluble when protonated. At the same time, by tuning the pH value during polymerization step the size of the cluster can be controlled. Larger, Au500 cluster favors slightly lower but still alkaline pH 9, and low MeOH concentration of 25%. Whereas, Au250 was synthesized at pH 11 and the solvent mixture of 28% (v/v) MeOH in water.

When dissolved in water the new products display different colors (yellowish, brownish, reddish) indicating that they have different sizes. The syntheses of both sizes produced mg-quantities (~7 mg) of solid material. Each reaction product was analyzed

using polyacrylamide gel electrophoresis (PAGE) and based on the initial size estimation they were assigned as Au250 and Au500, respectively.

Recently, Azubel and Kornberg reported that apart from the thiol-to-gold ratio the size and uniformity of *m*MBA gold particles is highly dependent on adjustment of pH.[37] In contrast to 4-MBA (*p*MBA), *m*MBA ligand induces different properties for the Au-nanocluster mainly due to the meta-position of the acidic group in the phenyl ring, thus resulting in dissimilar ligand orientation and geometry.[39] Nevertheless, smaller *m*MBA clusters of 68 and 144 gold atoms were synthesized at pH 13.[37] In case of 4-MBA clusters the $Au_{102}(pMBA)_{44}$ (Au102) is synthesized also at pH 13 and these larger ones Au250 and Au500 by lowering the pH from 11 to 9. The synthesis conditions for smaller water-soluble MBA-protected nanocluster seem to favor high pH condition.

Table 1. Synthesis protocols of pMBA-protected gold nanoclusters. The values in columns 2nd, 3rd, 7th correspond to the molar ratios.

	polymerization				reduction		purification
Nanoclusters	*p*MBA	$HAuCl_4$	MeOH %	pH	MeOH %	$NaBH_4$	MeOH %

Au102	3	1	47	13	47	1.1	60
Au250	6	1	28	11	26	1.8	pure product without fractional precipitation
Au500	6	1	25	9	25	1.8	25

3.2. Characterization of AuMPCs. The size range information of the crude product was preliminarily acquired from their mobility in PAGE gel (Figure 2). The size information and number of gold atoms per product were further examined with HR-TEM. Determined Au contents were further used for estimating number of ligands by thermogravimetry. With UV-vis spectroscopy new insight into size-dependent evolution of surface plasmon resonance (Figure 3) was obtained. Powder X-ray diffraction (PXRD) technique was used to validate the structural features that were obtained by HR-TEM. Finally, based on all the gathered data about the size, symmetry, molecular composition and structure of these clusters, computational prediction was developed for representing structural features of water-soluble *p*MBA-protected Au250 and Au500 nanoclusters.

PAGE Dispersity and the size of the prepared AuMPCs were compared to the reference cluster $Au_{102}(p\text{MBA})_{44}$ (Figure 1 and S1). The products formed by wet-chemistry approach showed up as a single well-defined band in PAGE indicating monodispersity of AuMPCs. The particles were initially analyzed by determination of electrophoretic mobility. Both products had lower mobility than $Au_{102}(p\text{MBA})_{44}$ in the same PAGE run indicating larger sized clusters. Using Au102 as a reference sample, retention factors (r_f) were determined to be 0.77 and 0.64 for Au250 and Au500, respectively. The products possess stability both in solid and in solution at room temperature for at least six months, as determined by PAGE and UV-vis analysis.

Figure 1. PAGE bands of the Au102, Au250 and Au500 nanoclusters.

HR-TEM images of the AuMPCs were acquired by Gatan software, which was also used to determine diameter of selected particles (Figure 2 and S2, S3, S4). The biggest challenge in HR-TEM measurements is it interpretation due to the number of interferences (and low signal-noise ratio when measuring at atomic resolution). Therefore, edge-to-edge particle size determination is often difficult. The diameters in the figure 2 correspond to the maximum limit of the size, in other words, the size with error limit 0.1 nm. We estimated the diameter of the smaller product to be 1.7±0.1 nm, which fits to our previously reported size estimation[25] that was based on Gaussian fit from low-resolution TEM images, yielding the diameter in range of 1.6±0.3 nm (Figure 2a). The metal core diameter of the larger product was determined to be 2.2±0.1 nm (Figure 2b, S4).

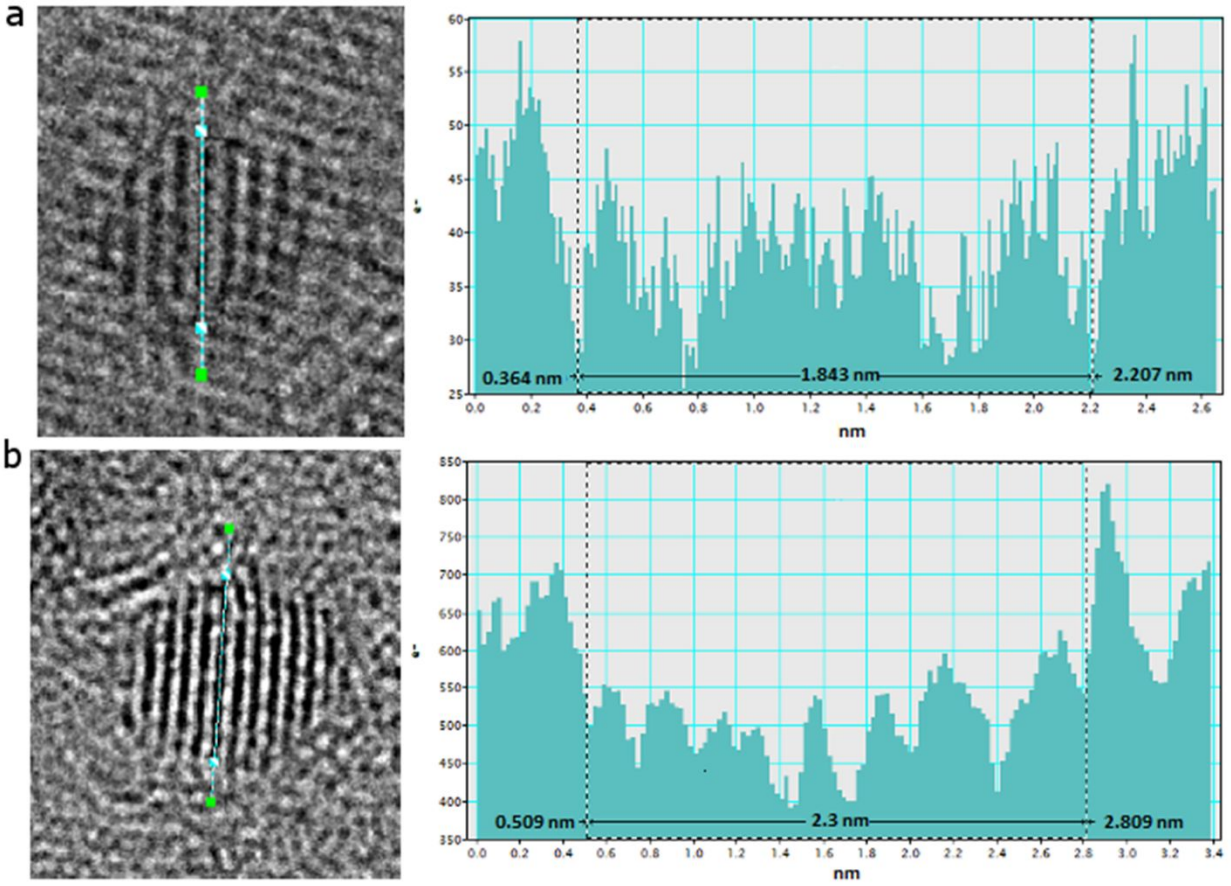

Figure 2. HR-TEM images of the assumed a) Au250 and b) Au500 *p*MBA-protected nanoclusters. Right panel corresponds to the histogram showing the upper size of the selected particle on the left panel.

UV-vis The optical spectra obtained from the two clusters were also compared to the reference spectrum of $Au_{102}(pMBA)_{44}$ (Fig. 3). In contrast to the $Au_{102}(pMBA)_{44}$, both clusters exhibited an absorption peak at 530 nm which is consistent to the surface plasmon resonance (SPR).[23] With an increase in cluster size, the SPR features

increase. The same properties were observed in case of Au250 and Au500 clusters. As far as we know, prepared particles are the biggest water-soluble nanoclusters synthesized by direct chemical approaches and demonstrating SPR. The spectrum of Au250 is compatible to the recently published spectra of 51 kDa,[33] 45 kDa[23] and 53 kDa clusters,[23] with the estimated number of gold atoms at 250, 226, and 253, respectively. In case of Au500, the absorption spectrum is compatible with reported spectra of 75 kDa[23] and 88 kDa clusters [33] with estimated gold atoms at 356 and 459.

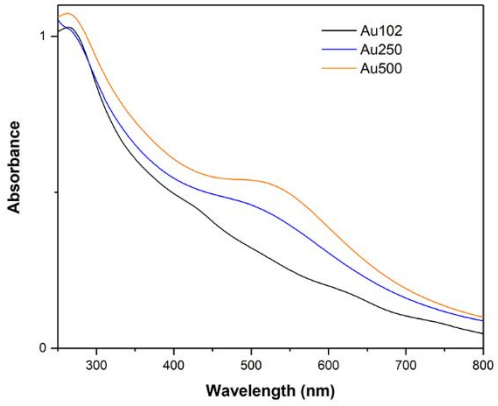

Figure 3. UV-vis spectra of Au102 (black), Au250 (blue) and Au500 (orange) clusters in dH_2O. A distinct absorption feature corresponding to a LSPR is observed at 530 nm for the Au250 and Au500 nanoclusters.

^{1}H NMR. ^{1}H spectrum of Au250 and Au500 exhibit a typical broad signal for gold clusters between 5.2 - 9.2 ppm (Figure S5). Additionally two sharp signals (doublets) can be seen at 7.60 and 7.79 ppm in both spectra, which fit to free *p*MBA-ligand. However, the ^{1}H spectrum of Au500 shows additional fine structure in comparison to Au250, which is relatively featureless. Without considering the free *p*MBA signals, the Au500 spectrum shows 14 doublet signals (7.92, 7.82, 7.70, 7.65, 7.34, 7.30, 7.14, 6.66, 6.62, 6.55, 6.51, 6.25, 6.19 and 5.79 ppm) and a singlet at 7.61 ppm. These peaks are characteristic for Au500 nanocluster, but it is still not clear whether they belong to the cluster structures. In different synthesis products, they appear at the same positions, but with varying intensities.

Thermogravimetric analysis (TG). The weight loss of organic substance upon heating is commonly used to estimate the number of ligands in monolayer protected gold clusters (the image of the Au residuals after a TG run, see S6). Thermal stability and number of organosulfur ligands on the Au_n nanoclusters (n = 102, 250, 500) were

examined by thermogravimetric analyses (TG). In figure 4, recorded TG curves show gently descending weight loss (sample dependently 0.4 – 2 wt.-%) from 20 up to about 200 °C (Table 2) that is caused by gradual evaporation of residual surface bound water. Thermal decomposition of all three Au-clusters initiate slowly above 220 °C followed by major weight loss from 270 °C to 500, 600 and 700 °C along with an increase in the size of the Au-cluster. The observed weight losses of the major steps correspond to thermal decomposition processes and/or desorption of surface ligands (*p*MBA), and were determined to be 25.92, 21.32 and 19.60 wt.-% for Au102, Au250 and Au500 clusters, respectively (Table 2).

The number of surface ligands can be estimated via the observed residual weight of each TG run (74.08, 78.68, and 83.11% for Au102, Au250 and Au500, respectively) by calculating those as moles of Au. The number of gold atoms used here are based on computationally aided predictions explained in detail later in the section 3.4. The original molar mass of the $Au_x(SR)_y$ cluster can then be calculated based on the expected 1 to 1 stoichiometry between the gold containing residual and the original $Au_x(SR)_y$ cluster, from which the number of surface ligands $(SR)_y$ can then be evaluated by taking into

account the molar mass of the (SR) ligand. Functionality of the method was confirmed by the reference cluster Au102 for which 45 ±1 surface ligands is determined by the analysis, agreeing well to number of the ligands (44) reported in the single crystal structure of the cluster by Jadzinsky *et al.*[45] Similarly, 73-80 and 111-116 surface ligands were determined for Au250 and Au500 clusters, respectively. Determined number of ligands match also remarkably well to those obtained by our computational predictions (see section 3.4).

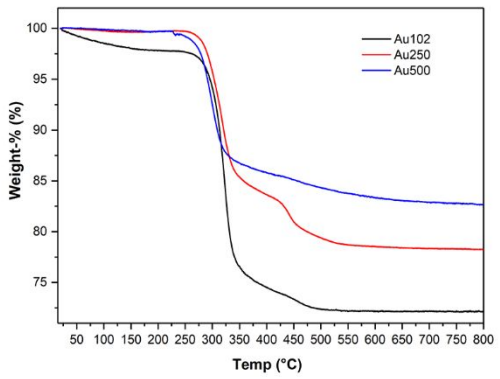

Figure 4. TG curves of Au102, Au250 and Au500 clusters measured with a heating rate of 10 °C/min under air atmosphere.

Table 2. TG results for Au102, Au250 and Au500 nanoclusters.

Sample name	1st weight loss [a] (%)	Temp. (°C)	2nd weight loss [b] (%)	Temp. (°C)	Residual [c] (%)	No. of ligands	No. of Au atoms
Au102	2.13	24 - 214	25.92	214 - 800	74.08	45	102
Au250	0.37	24 - 190	21.32	190 - 800	78.68	73 - 80	210 - 230
Au500	0.40	24 - 192	16.90	192 - 800	83.11	111 - 116	426 - 442

a = residual water, b = ligand removal, c = residual weight corresponding to gold content

Toxicity on bacteria Neither Au250 nor Au500 caused significant decrease or elevation in the growth densities of *Bacillus thuringiensis* HER1410, *Escherichia coli* HB101 or *Klebsiella pneumoniae* in concentrations 0.14 – 14 μg/ml of Au250 or 0.13 – 13 μg/ml of Au500 (Figure 5). In higher concentrations (140 μg/ml and 130 μg/ml) the self-absorption of Au250 and Au500 obscured the optical density of the cultures and thus the changes in bacterial growth could not be reliably observed. Nevertheless, based on the results, Au250 and Au500 do not seem to affect bacterial viability.

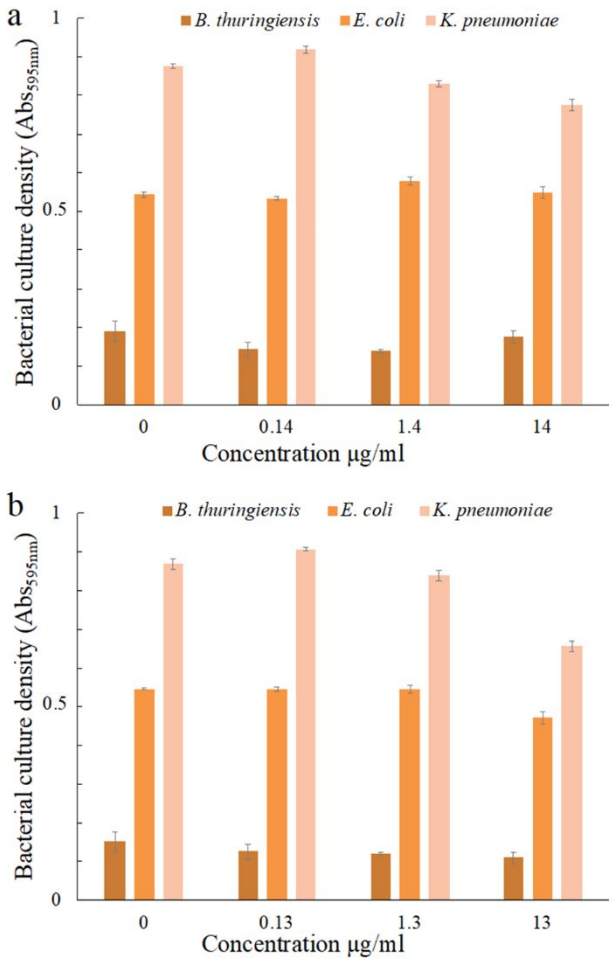

Figure 5. Spectroscopic biotoxicity assay of gold nanoclusters a) Au250 and b) Au500 on bacterial species *Bacillus thuringiensis*, *Escherichia coli* and *Klebsiella pneumoniae*. Maximum absorption (595 nm) of bacterial cultures were measured in the presence of either Au250 or Au500 in different concentrations during 20 h cultivation (N=3). The slight decline of absorbance in the highest concentration was due to increasing background absorption. Error bars: standard deviation.

3.3. Exploring the atomic structure

Before predicting the molecular compositions of the clusters, we first present a short discussion on the structural patterns of water-soluble *p*MBA-protected cluster systems. We compare measured powder X-ray diffraction results of the synthesized clusters to the symmetries of selected, structurally known, thiolate protected clusters. We also present a range for possible basis for metal core structure of Au250 and Au500 nanoclusters based on experimental and theoretical data.

Powder X-ray diffraction (PXRD) analysis

Comparison of the experimental XRD patterns of Au250 and Au500 nanoclusters to the calculated reference systems of $Au_{146}(pMBA)_{57}$, $Au_{246}(SC_6H_4CH_3)_{80}$ and $Au_{279}(TBBT)_{84}$ is illustrated in Figure 6. The Au_{246} nanocluster displays the decahedral core and $Au_{146}(pMBA)_{57}$ represents the largest so far solved water-soluble cluster with FCC-based twinned core.[41] The XRD patterns of both clusters show the strongest diffraction peak at ~40° 2θ, two relatively broad peaks at ~60 - 80° 2θ and some minor peaks at ~45° and ~50° 2θ. With phase identification routine, the observed diffraction

peaks are characteristic for gold phase crystallizing in cubic face-centered crystal system and no additional unindexed peaks remain in the patterns (large hump 15 - 20° and very sharp peak at 21.4° 2θ originates from a sample holder/adhesive substance)[43]. The calculated XRD pattern of $Au_{146}(p\text{MBA})_{57}$ is remarkably similar to the experimental data of Au250 and Au500 clusters. As the diffraction peaks at 38.8°, 66.2° and 75.7° in both experimental patterns have similar shape features and are located at the equal diffraction angles than that of in Au146 pattern. Instead, the simulated patterns of decahedral Au246 and FCC Au279 cluster show additional minor peaks at ~45° and ~50° 2θ that are not visible in the XRD patterns of Au500 and Au250 clusters. Moreover, the peak maximums of the main peaks in Au246 and Au279 are also somewhat shifted to lower 2θ angles and the shape properties of the peaks are subtlety different. Described observations suggest that the metal core of both Au250 and Au500 nanoclusters most likely adopts the FCC symmetry, which is also twinned as indicated by the computational analyses represented in following chapters.

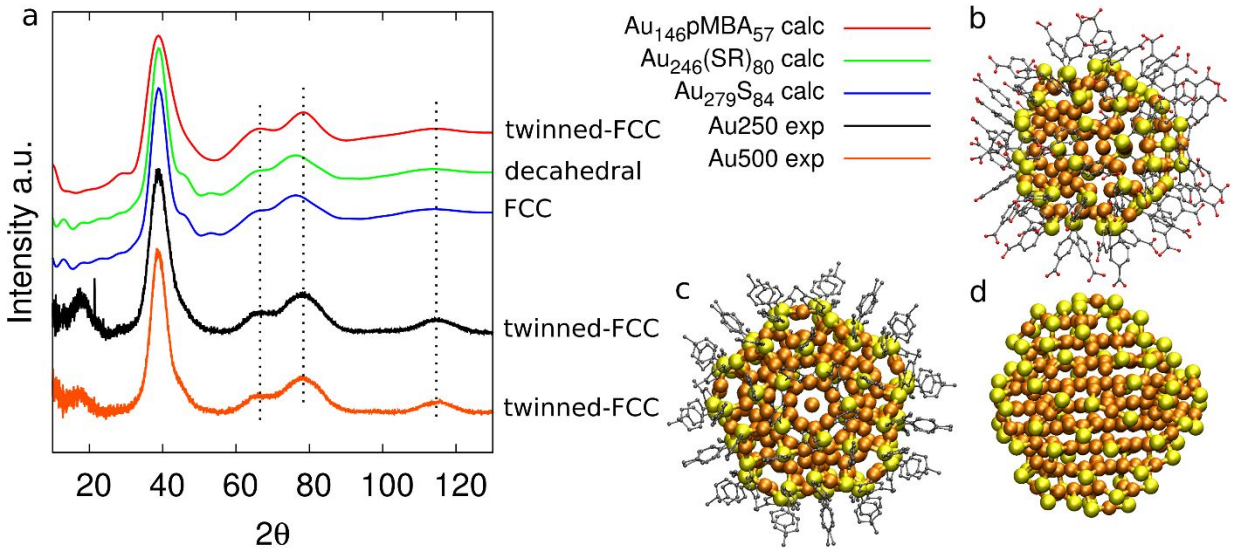

Figure 6. a) Diffraction patterns of the nanoclusters. Comparison of the experimental patterns of Au250 (black line) and Au500 (orange line) to the calculated patterns of Au146, Au246, and Au279 clusters. The diffraction hump and very sharp peak at 20° 2θ in experimental patterns are caused by the sampler holder and the adhesive used for attaching the samples to the holder. Structural models of b) $Au_{146}(pMBA)_{57}$ c) $Au_{246}(SR)_{8}$ and d) $Au_{279}S_{84}$.

Building model for twinned FCC metal core structures of Au250 and Au500

Based on the obtained information from powder XRD analysis we start evaluating possible basis for metal core structure of Au250 and Au500 nanoclusters. Ranges of

possible candidates with the same twinned-FCC arrangement are shown in Figure 7. The size range of the clusters was estimated based on PAGE. Furthermore, the estimated diameters of the clusters from HR-TEM, 1.7±0.1 nm for Au250 and 2.2±0.1 nm for Au500 are in agreement with modelled metal core of Au_{201} and Au_{405}, respectively. Therefore, we believe that they are possible candidates to start building structural model of the synthesized clusters.

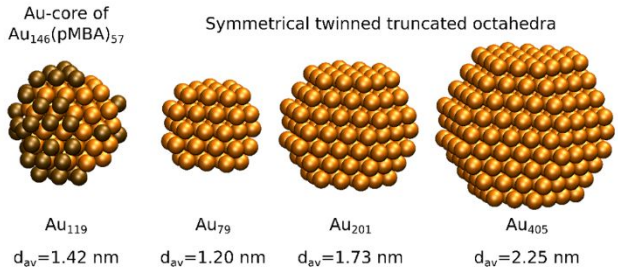

Figure 7. The range for possible basis for metal core structure in twinned FCC octahedral arrangement. Orange color represents gold atoms and brown color represents the additional layer of atoms on top of symmetrical Au_{79} (left) representing together the Au-core of $Au_{146}(p\text{MBA})_{57}$.

HR-TEM image versus twinned-FCC core

HR-TEM images represent further the symmetries of the AuMPCs. The simulated HR-TEM images of Au_{201} metal core clearly support the imaging experiments of Au250 (Figure 8). The observation of the lattice fringes in Figure 8 c) clearly shows the effects that can be only seen in both, FCC and twinned-FCC arrangements. The experimental figure 8 c) shows 7-9 rows of atomic layer giving excellent estimation of structural information at atomic resolution. The uncertainty in image interpretation is often due to poor contrast and number of interferences. Therefore, we simulated images of Au_{201} metal core and compared them with our experimental findings. In the simulated image, there are 7 rows of the atomic layer (Fig. 8 c). The simulated images contain only the metal core atoms and the question arises how protected is the gold core under electron beam. In other words, for the analysis it is important to know whether the Au-S layer protecting the gold core is visible in the HR-TEM images. Simulated HR-TEM images and experimental equivalents Figure 8 a), b), d) show the effects that are reproducible only with the stacking fault defect for FCC-symmetry. Nevertheless, the symmetry found from powder XRD and HR-TEM are the same, which indicates that the core structure will remain the same under electron beam.

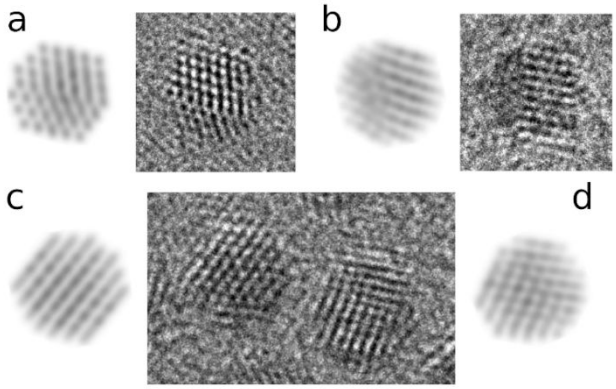

Figure 8. Comparison of HR-TEM images of Au250 and simulated images of Au201 metal core from different directions.

3.4. Predicting molecular composition

There is enough complementary experimental information for attempting determination of the molecular composition of the investigated clusters. Herein, we provide computationally aided predictions for the molecular compositions by reflecting the measured results of the synthesized clusters to the properties of selected, structurally known, thiolate protected clusters of a similar size. Selected known reference systems include clusters with close to spherical shape such as $Au_{102}(p\text{MBA})_{44}$, $Au_{146}(p\text{MBA})_{57}$, $Au_{246}(SC_6H_4CH_3)_{80}$ and $Au_{271}(TBBT)_{84}$, matching the

overall shape of the synthesized *p*MBA-protected particles. The clusters are selected from the size range from 100 - 300 including the two known *p*MBA-clusters. Due to the absence of experimentally resolved structures of larger size water-soluble clusters, we included two of the largest thiolate protected clusters, despite of them being protected with different type of aromatic ligands.

By assuming *p*MBA-ligand for the selected known cluster compositions, trends of theoretical TG weight loss percentages can be predicted with the respect to the number of Au-atoms and the number of ligands as shown in Figure 9. Behavior shown in the figure is quite monotonous and by assuming that the behavior is valid also for the synthesized clusters, the composition $Au_{210}(pMBA)_{72}$ can be predicted for the smaller cluster. Noteworthy is, that this composition would match perfectly with the magic electron shell closing of spherical clusters at 138 e, by assuming that gold provides 210 Au(6s)-based free electrons to the system and the Au-*p*MBA bonding withdraws 72 electrons out from the system.[46]

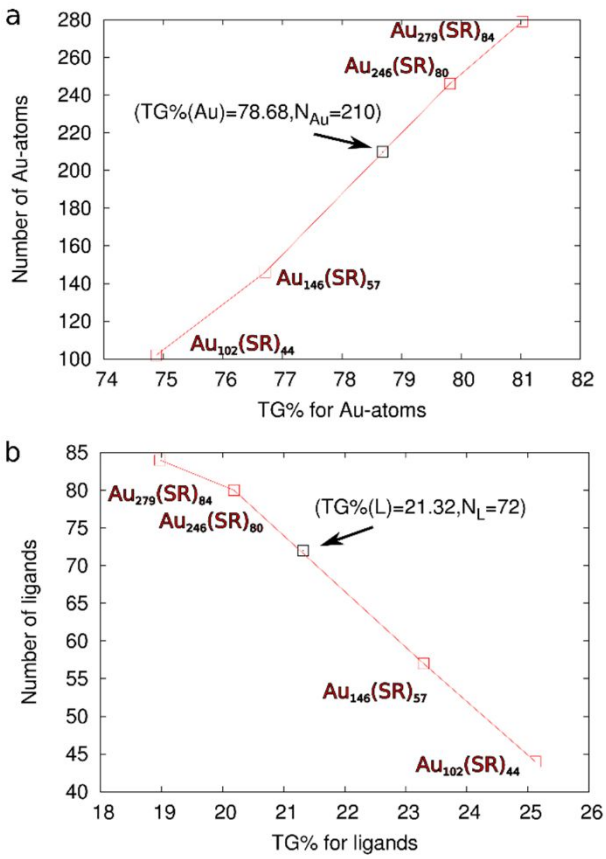

Figure 9. a) Number of Au-atoms in the thiolated clusters as a function of theoretically calculated thermogravimetric (TG) weight loss percentages of Au content. b) Number of ligands in the thiolated clusters as a function of theoretically calculated ligand TG percentages. Both are drawn using *p*MBA-ligand.

The second method for size estimation is based on the diameters of the clusters determined from the HR-TEM images the probable sizes of the metal core of the clusters can be estimated computationally. Figure 10 shows the number of metal atoms as a function of diameter as calculated for bare metal clusters of twinned-FCC symmetry. Model clusters were generated as described in Methods section. Using the

experimentally measured diameters, the two synthesized clusters have approximately 187±30 and 385±50 Au-atoms in their metal cores based on the correlation shown in Figure 10. The number of metal atoms in the Au-S interface varies from 23 to 40 in case of the selected four known reference clusters. Assuming further that 30-40 Au-atoms would participate on protecting units, the smaller synthesized particle would have approximately 220-230 Au-atoms in total depending on the actual Au-S interface conformation. Furthermore, we can estimate that at least 40 Au-atoms should be contributing to the Au-S interface of the larger synthesized cluster increasing the size to >425 Au-atoms in total.

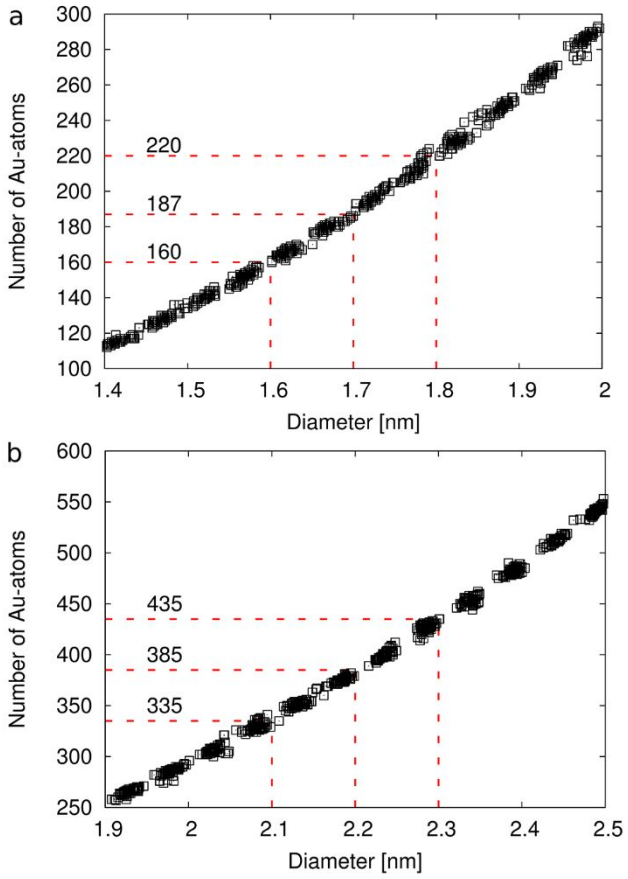

Figure 10. Number of Au-atoms of the spherical bare twinned-FCC Au-clusters in the size range relevant for the investigated *p*MBA-clusters in a) and b). The plausible sizes 187 and 385 of the metal core for the measured diameters are labeled in the figure. Based on the 0.1 nm error limits the minimum and maximum values are also given.

Third, we did linear fitting on the properties of the selected known clusters. We correlated the diameter of the cluster including metal core and Au-S interface to the

number of gold atoms in the cluster as shown in Figure 11 a). We also correlated the number of ligands in the cluster to the spherical surface area as shown in Figure 11 b). The two linear correlations can be used to predict the molecular composition by relying on experimentally measured diameters or on the estimated total number of gold atoms in the synthesized clusters.

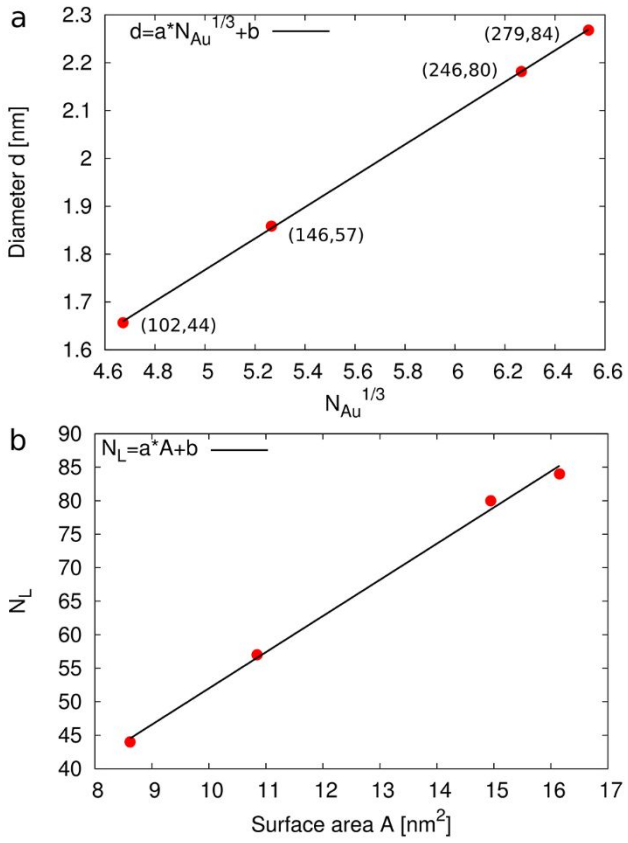

Figure 11. a) Linear fitting done by correlating the number of Au-atoms in the cluster to the diameter of the cluster taking into account the metal core and Au-S interface atoms

and b) by correlating the corresponding spherical surface area to the number of ligands. Fitted parameters: a) a = 0.328 nm, b = 0.129 nm and b) a = 5.40 nm^{-2}, b = -2.02. Diameters of the clusters are determined including Au-core and Au-S interface as described in Methods section.

For the smaller Au250 cluster the size range from 210-230 Au-atoms was already estimated to be realistic. Fixing the number of gold atoms to 210 gives as a prediction 2.1 nm diameter for the cluster (including the metal core and the Au-S interface) and further 71 ligands for the protecting layer. Both are in agreement with the experimentally measured results. For example, the 1.7 nm diameter of the metal core should be increased at maximum twice the Au-S bond (0.235 nm) when adding the metal ligand interface. With the same procedure the upper size limit for the number of gold atoms at 230 gives a prediction of 2.1 nm diameter and 75 ligands, for which the closest composition matching the measured TG-percentages would be $Au_{230}(p\text{MBA})_{80}$.

For the larger Au500 cluster prediction of the molecular composition can be also made although the reliability is not equally good due to the lack of reference structures.

For the larger cluster we take the measured diameter 2.2 nm of the core and add to it approximately 0.4 nm from the metal-ligand interface. For the 2.6 nm spherical particle correlations predict that the total number of Au-atoms should be 429 and the number of ligands 113. Molecular composition would be $Au_{429}(SR)_{113}$ which has a very good match with the measured TG weight loss percentages. All the nearby compositions within 0.1 TG-percentage units from the measured results are included in compositions $Au_{426-442}(p\text{MBA})_{112-115}$. The prediction of 426-442 gold atoms in total is reasonable as compared to the estimated core size of 385 Au-atoms, which would mean that 40-60 Au-atoms were included in the protecting units. The number of single bridged ligands, not resembling a conformation of any protecting unit, increases in the Au-S interface as the cluster size increases. This can be realized by analyzing the structures of the known reference clusters $Au_{102}(SR)_{44}$, $Au_{146}(SR)_{57}$, $Au_{246}(SR)_{80}$ and $Au_{279}(SR)_{84}$. Their Au-S interfaces include respectively 0% (0/44), 12.3% (7/57), 12.5% (10/80) and 21.4% (18/84) of bridged ligands. At the same time the relative number of Au-atoms in the Au-S interface decreases as the cluster size increases, at least within the represented size range.

As a summary, the best computationally aided predictions for the molecular compositions are $Au_{210-230}(p\text{MBA})_{70-80}$ for the smaller cluster and $Au_{426-442}(p\text{MBA})_{112-115}$ for the larger cluster.

4. CONCLUSION

In this work, we synthesized, in milligram scale, stable sizes of water-soluble *p*MBA-protected gold nanoclusters by controlling the pH in different MeOH/H_2O conditions. The products were carefully analyzed by various analytical techniques and characterized for approximate mass and structural composition. So far, water-soluble clusters have been observed in decahedral (Au_{102}(*p*MBA)$_{44}$),[45] FCC-like (Au_{68}(*m*MBA)$_{32}$ and Au_{144}(*m*MBA)$_n$)[38] and twinned-FCC (Au_{146}(*p*MBA)$_{57}$) symmetries[41]. The results in this paper indicate that twinned-FCC symmetry is favored in larger *p*MBA-protected clusters as shown in the case of Au250 and Au500. Combining all the experimental information and computational analysis we came to the final prediction of the molecular composition of the synthesized clusters, namely $Au_{210\text{-}230}$(*p*MBA)$_{70\text{-}80}$ and $Au_{426\text{-}442}$(*p*MBA)$_{112\text{-}115}$. The structural knowledge of these clusters is crucial when applying these to biological studies. There is still a lack of well-defined, water-soluble particles, which could serve as universal labeling tools for bioimaging. Attaching gold

nanoclusters to the biological systems will allow the investigation of viruses, including their entry mechanism into cells. The development of cluster-based sensors by chemically modifying the ligand layer of the water-soluble gold nanoclusters is one of the possibilities to achieve controllable application in biosciences and to study for example the nature of viral genome release in cells (during infection). In addition, in the field of spectroscopy in physical chemistry, the plasmonic nanoclusters are important model systems to study emergence of bulk properties in metal and using them as a building blocks could give deepen understanding of energy transfer processes, which are of interest in molecular electronics.

This work introduces some overall trends in synthetic methods and structural compositions for two larger water-soluble AuMPCs. These play a crucial role in understanding the relation of their diverse properties and increase the usability of gold nanoclusters.

ASSOCIATED CONTENT

Supporting Information. Supporting Information is available free of charge on the ACS Publications website at DOI

Detailed experimental procedures and methods for prediction of molecular composition; PAGE gel showing fractional precipitation procedure; TEM images taken from Au250 and Au500 nanoclusters; full spectrum of ^{1}H NMR of Au250 and Au500 nanoclusters; Image of the residual after TG run. This material is available free of charge via the Internet at http:

AUTHOR INFORMATION

Corresponding Author

*E-mail: tanja.m.lahtinen@jyu.fi. Phone: +358 40805 3697 (T.L.).

ORCID

Tanja Lahtinen: 0000-0002-1747-6959; Hannu Häkkinen: 0000-0002-8558-5436

Notes

The authors declare no competing financial interest.

ACKNOWLEDGMENT

We acknowledge Aalto University for the access to HR-TEM facilities and technical support.

Funding Sources

This work was financially supported by the Academy of Finland via projects 269402, 273499, 303753 (L.L.), 252411, 297049, 292352 (H.H.), 294217 (H.H), and Emil Aaltonen Foundation grant to M.J.

REFERENCES

(1) Salorinne, K.; Lahtinen, T.; Malola S.; Koivistoa, J.; Häkkinen, H. Solvation Chemistry of Water-Soluble Thiol Protected Gold Nanocluster Au102 from DOSY NMR Spectroscopy and DFT Calculations. *Nanoscale* **2014**, *6*, 7823.

(2) Plascencia-Villa, G.; Demeler, B.; Whetten, R.L.; Griffith, W.P.; Alvarez, M.; Black, D.M.; José-Yacamán, M. Analytical Characterization of Size-Dependent Properties of Larger Aqueous Gold Nanoclusters. *J. Phys. Chem. C* **2016**, *120*, 8950−8958.

(3) Jin, R. Atomically precise metal nanoclusters: stable sizes and optical properties. *Nanoscale* **2015**, *7*, 1549.

(4) Marjomäki, V.; Lahtinen, T.; Martikainen, M.; Koivisto, J.; Malola, S.; Salorinne, K.; Pettersson, M.; Häkkinen, H. *Proc. Natl. Acad. Sci.* U. S. A., **2014**, *111*, 1277–1281.

(5) Homberger, M.; Simon, U. On the Application Potential of Gold Nanoparticles in Nanoelectronics and Biomedicine. *Philos. Trans. R. Soc., A* **2010**, *368*, 1405−1453.

(6) Nie, S.; Emory, S. R. Probing Single Molecules and Single Nanoparticles by Surface- Enhanced Raman Scattering. *Science* **1997**, 275, 1102−1106.

(7) Brongersma, M. L.; Halas, N. J.; Nordlander, P. Plasmon-Induced Hot Carrier Science and Technology. *Nat. Nanotechnol*. **2015**, *10*, 25− 34.

(8) Tapio, K.; Leppiniemi, J.; Shen, B.; Hytönen, V. P.; Fritzsche, W.; Toppari, J. J. Toward Single Electron Nanoelectronics Using Self- Assembled DNA Structure. *Nano Lett.* **2016**, *16*, 6780−6786.

(9) Martikainen, M.; Salorinne, K.; Lahtinen, T.; Malola, S.; Permi, P.; Häkkinen, H.; Marjomäki, V.; Hydrophobic pocket targeting probes for enteroviruses. *Nanoscale* **2015**, *7*, 17457.

(10) Stark, M.C.; Baikoghli, M.A.; Lahtinen, T.; Malola, S.; Xing, L.; Nguyen, M.; Nguyen, M.; Sikaroudi, A.; Marjomäki, V.; Häkkinen, H.; et al. Structural Characterization of Site-Modifed Nanocapsid with Monodispersed Gold Clusters. *Scientific Reports* **2017**, *7*, 1-11.

(11) Calard, F.; Wani, I.H.; Hayat, A.; Jarrosson, T.; Lère-Porte, J.-P.; Jafri, S.H.M.; Serein-Spirau, F.; Leifer, K.; Orthaber, A. Designing Sterically Demanding Thiolate Coated AuNPs for Electrical Characterization of BPDT in a NP–Molecule–Nanoelectrode Platform. *Mol. Syst. Des. Eng*. **2017**, *2*, 133.

(12) Häkkinen, H. The Gold-Sulfur Interface at the Nanoscale. *Nat. Chem.*, **2012**, *4*, 443–455.

(13) Jin, R.; Zeng, C.; Zhou M.; Chen, Y. Atomically Precise Colloidal Metal Nanoclusters and Nanoparticles: Fundamentals and Opportunities. *Chem. Rev.* **2016**, *116*, 10346–10413.

(14) Chakraborty, I.; Pradeep, T. Atomically Precise Clusters of Noble Metals: Emerging Link between Atoms and Nanoparticles. *Chem. Rev.* **2017**, *117*, 8208–8271.

(15) Sakthivel, N.A.; Theivendran, S; Ganeshraj, V.; Oliver, A.G.; Dass, A. Crystal Structure of Faradaurate-279: $Au_{279}(SPh\text{-}tBu)_{84}$ Plasmonic Nanocrystal Molecules. *J. Am. Chem. Soc.* **2017**, *139*, 15450-15459.

(16) Kumara, C.; Zuo, X.; Ilavsky, J.; Chapman, K.-W.; Cullen, D.-A.; Dass, A. Super-Stabile Highly Monodisperse Plasmonic Faradaurate-500 Nanocrystals with 500 Gold Atoms: $Au_{\sim 500}(SR)_{\sim 120}$. *J. Am. Chem. Soc.* **2014**, *136*, 7410-7417.

(17) Jin, R.; Qian, H.; Wu, Z.; Zhu, Y.; Zhu, M.; Mohanty, A.; Garg, N. Size Focusing: A Methodology for Synthesizing Atomically Precise Gold Nanoclusters. *J. Phys. Chem. Lett.*, **2010**, *1*, 2903–2910.

(18) Qian, H.; Zhu, Y., Jin, R. Size-Focusing Synthesis, Optical and Electrochemical Properties of Monodisperse $Au_{38}(SC_2H_4Ph)_{24}$ Nanoclusters. *ACS Nano* **2009**, *3*, 3795−3803.

(19) Qian, H.; Zhu, Y., Jin, R. Atomically Precise Gold Nanocrystal Molecules with Surface Plasmon Resonance. *Proc.Natl.Acad.Sci.U.S.A.* **2012**, *109*, 696−700.

(20) Qian, H.; Jin, R. Ambient Synthesis of $Au_{144}(SR)_{60}$ Nanoclusters in Methanol. *Chem. Mater.* **2011**, *23*, 2209−2217.

(21) Schaff, T.; Whetten, R. Controlled Etching of Au:SR Cluster Compounds. J. Phys. Chem. B **1999**, *103*, 9394−9396.

(22) Dharmaratne, A. C.; Krick, T.; Dass, A. Nanocluster Size Evolution Studied by Mass Spectrometry in Room Temperature $Au_{25}(SR)_{18}$ Synthesis. *J. Am. Chem. Soc.* **2009**, *131*, 13604−13605.

(23) Negishi, Y.; Nakazaki, T.; Malola, S.; Takano, S.; Niihori, Y.; Kurashige, W.; Yamazoe, S.; Tsukuda T.; Häkkinen, H. A Critical Size for Emergence of Nonbulk Electronic and Geometric Structures in Dodecanethiolate-Protected Au Clusters. *J. Am. Chem. Soc.* **2015**, *137*, 1206–1212.

(24) Yi, C.; Zheng, H.; Tvedte, L.M.; Ackerson, C.J.; Knappenberger, K.L.J. Nanometals: Identifying the Onset of Metallic Relaxation Dynamics in Monolayer-Protected Gold Clusters Using Femtosecond Spectroscopy. *J. Phys. Chem. C* **2015**, *119*, 6307– 6313.

(25) Lahtinen, T.; Hulkko, E.; Sokołowska, K.; Tero, T.-R.; Saarnio, V.; Lindgren, J.; Pettersson, M.; Häkkinen, H.; Lehtovaara, L. Covalently Linked Multimers of Gold Nanoclusters $Au_{102}(p\text{MBA})_{44}$ and $Au_{\sim 250}$ $(p\text{MBA})_n$. *Nanoscale* **2016**, *8*, 18665−18674.

(26) Yampolsky, S.; Fishman, D.A.; Dey, S.; Hulkko, E.; Banik, M.; Potma, E.O.; Apkarian, V.A. Seeing a Single Molecule Vibrate Through Time-Resolved Coherent Anti-Stokes Raman Scattering. *Nature Phot.* **2014**, *8*, 650.

(27) Sels, A.; Salassa, G.; Cousin, F.; Lee, L.-T.; Bürgi, T. Covalently Bonded Multimers of $Au_{25}(SBut)_{18}$ as a Conjugated System. *Nanoscale* **2018**, *10*, 12754.

(28) Schaaff, T.; Knight, G.; Shafigullin, M.; Borkman, R.; Whetten, R. Isolation and Selected Properties of a 10.4 kDa Gold:Glutathione Cluster Compound. *J. Phys. Chem. B* **1998**, *102*, 10643−10646.

(29) Schaaff, T.; Whetten, R. Controlled Etching of Au:SR Cluster Compounds. *J. Phys. Chem. B* **1999**, *103*, 9394−9396.

(30) Dass, A. Faradaurate Nanomolecules: A Superstable Plasmonic 76.3 kDa Cluster. *J. Am. Chem. Soc.*, **2011**, *133*, 19259–19261.

(31) Alvarez, M.M.; Chen, J.; Plascencia-Villa, G.; Black, D.M.; Griffith, W.P.; Garzon, I.L.; Jose-Yacaman M.; Demeler, B.; Whetten, R.L. Hidden Components in Aqueous

"Gold-144" Fractionated by PAGE: High-Resolution Orbitrap ESI-MS Identifies the Gold-102 and Higher All-Aromatic Au-pMBA Cluster Compounds. *J. Phys. Chem. B* **2016**, *120*, 6430−6438.

(32) Plascencia-Villa, G.; Demeler, B; Whetten, R.L.; Griffith, W.P.; Alvarez, M.; Black, D.M.; Jose-Yacaman, M. Analytical Characterization of Size-Dependent Properties of Larger Aqueous Gold Nanoclusters. *J. Phys. Chem. C* **2016**, *120*, 8950−8958.

(33) Tvedte, L.M.; Ackerson, C.J. Size-Focusing Synthesis of Gold Nanoclusters with *p*-Mercaptobenzoic Acid. *J. Phys. Chem. A* **2014**, *118*, 8124−8128.

(34) Levi-Kalisman, Y.; Jadzinsky, P. D.; Kalisman, N.; Tsunoyama, H.; Tsukuda, T.; Bushnell, D. A.; Kornberg, R. D. Synthesis and Characterization of $Au_{102}(p\text{MBA})_{44}$ Nanoparticles. *J. Am. Chem. Soc.* **2011**, *133*, 2976−2982.

(35) Ackerson, C. J.; Jadzinsky, P. D.; Sexton, J. Z.; Bushnell, D. A.; Kornberg, R. D. Synthesis and Bioconjugation of 2 and 3 nm-Diameter Gold Nanoparticles. *Bioconjugate Chem.* **2010**, *21*, 214−218.

(36) Wong, O.A.; Compel, W.S.; Ackerson, C.J. Combinatorial Discovery of Cosolvent Systems for Production of Narrow Dispersion Thiolate-Protected Gold Nanoparticles. *ACS Comb. Sci.* **2015**, *17*, 11−18.

(37) Azubel, M.; Kornberg, R.D. Synthesis of Water-Soluble, Thiolate-Protected Gold Nanoparticles Uniform in Size. *Nano Lett.* **2016**, *16*, 3348−3351.

(38) Azubel, M.; Koivisto, J.; Malola, S.; Bushnell, D.; Hura, G.L.; Koh, A.-L.; Tsunoyama, H.; Tsukuda, T.; Pettersson, M.; Häkkinen, H.; et al. Electron Microscopy of Gold Nanoparticles at Atomic Resolution. *Science* **2014,** *6199*, 909-912.

(39) Tero, T.-R.; Malola S., Koncz, B.; Pohjolainen, E.; Lautala, S.; Mustalahti, S.; Permi, P.; Groenhof, G.; Pettersson, M.; Häkkinen, H. Dynamic Stabilization of the Ligand–Metal Interface in Atomically Precise Gold Nanoclusters Au_{68} and Au_{144} Protected by *meta*-Mercaptobenzoic Acid. *ACS Nano* **2017**, *11*, 11872–11879.

(40) Azubel, M.; Koh, A.-L.; Koyasu, K.; Tsukuda, T.; Kornberg, R.-D. Structure Determination of a Water-Soluble 144-Gold Atom Particle at Atomic Resolution by Aberration-Corrected Electron Microscopy. *ACS Nano* **2017**, *11*, 11866–11871.

(41) Vergara, S.; Lukes, D.A.; Martynowycz, M.W.; Santiago, U.; Plascencia-Villa, G.; Weiss, S.C.; Cruz, M.J.; Black, D.M.; Alvarez, M.M.; López-Lozano, X.; et al. MicroED Structure of $Au_{146}(p\text{MBA})_{57}$ at Subatomic Resolution Reveals a Twinned FCC Cluster *J. Phys. Chem. Lett.*, **2017**, *8*, 5523–5530.

(42) Sokołowska, K.; Hulkko, E.; Lehtovaara, L.; Lahtinen, T. Dithiol-Induced Oligomerization of Thiol-Protected Gold Nanoclusters *J. Phys. Chem. C* **2018**, *122*, 12524–12533.

(43) International Centre for Diffraction Data, ICDD-PDF4+. http://www.icdd.com/ (accessed December 10, 2018).

(44) Lopez-Acevedo, O.; Akola, J.; Whetten, R.L.; Grönbeck, H.; Häkkinen, H. Structure and Bonding in the Ubiquitous Icosahedral Metallic Gold Cluster $Au_{144}(SR)_{60}$. *J. Phys. Chem. C* **2009**, *113*, 5035.

(45) Jadzinsky, P.D.; Calero, G; Ackerson, C.J.; Bushnell, D.A.; Kornberg, R.D. Structure of a Thiol Monolayer-Protected Gold Nanoparticle at 1.1 Å Resolution. *Science* **2007**, *318*, 430-433.

(46) Walter, M.; Akola, J.; Lopez-Acevedo, O.; Jadzinsky, P.-D.; Calero, G.; Ackerson, C.-J.; Whetten, R.-L.; Grönbeck, H.; Häkkinen, H.; A Unified View of Ligand-Protected Gold Clusters as Superatom Complexes. *Proc.Natl.Acad.Sci.U.S.A.* **2008**, *105*, 9157-9162.

TOC Graphic